Electron multipacting in RF structures

Erkki Somersalo[1] Pasi Ylä-Oijala[1] Dieter Proch[2]

[1]Rolf Nevanlinna Institute, University of Helsinki
[2] DESY, Hamburg

1 Introduction

Electron multipacting is one of the most important problems in superconducting RF cavities. This phenomenon affects the cavities in various ways, causing e.g. power losses in accelerator resonators, exessive heating of the walls and breaking of the ceramic windows. The multipacting is a resonant phenomenon, where the spontaneously emitted electrons are driven by the electromagnetic field and impacting the cavity wall. If the orbit is synchronous to the RF field, the electron impact may release secondary electrons and the number of the electrons on the synchronous trajectry is multiplied at each impact. This results very rapidly to a drastic increase of electron impacts at certain points. Basically two different multipacting mechanisms are described in literature ([1], [3], [4], [7]). In the first one, the model case is two parallel plates with oscillating voltage drop. The resonant electron trajectories bounce from one plate to another and back in a time of flight equal to an integer number of RF periods. In the second one, the electrons are driven by the magnetic field, the flight time being an integer times the synchrotron period. In this report, a systematic way of finding different and possibly new multipacting mechanisms is proposed. The electron trajectories are described as a discrete dynamical system in an appropriately chosen phase space. In this formulation, the occurrence of the multipacting phenomenon corresponds to fixed or multiply periodic points of the dynamical system. The general theory of dynamical systems seems to give potential methods of studying questions such as the stability of the resonant trajectories. This approach is applied to one model case, a coaxial line. The article [6] contains experimental results on multipacting in the coaxial geometry. Our method seems to be able to find new types of multipacting processes in this geometry.

2 The dynamical system

Let us first review the equations describing the dynamics of a relativistic electron in an electromagnetic field. Let Ω be a void cavity where a time harmonic electromagnetic field is supported. The electric field and the magnetic induction are denoted by $\vec{E}(x,t)$

and $\vec{B}(x,t)$. Assume that the wall of Ω, denoted as $\partial\Omega$, emits free electrons into Ω at a rate characteristic to the material of the wall. Assuming that the effect of the field of the electron itself on the external field is negligible, the dynamics is generated by the equations

$$\begin{cases} \dfrac{d\vec{v}}{dt} = -\dfrac{e}{m}\left(1-\left(\dfrac{v}{c}\right)^2\right)^{1/2}\left(\vec{E}+\vec{v}\wedge\vec{B}-\dfrac{1}{c^2}(\vec{v}\cdot\vec{E})\vec{v}\right)\,, \\ \dfrac{d\vec{x}}{dt} = \vec{v}\,, \end{cases} \tag{1}$$

where $\vec{v}$ is the 3–velocity of the electron, $v=|\vec{v}|$,and $-e$ and m are the charge and rest mass of the electron, respectively, and c is the speed of light in vacuum (see eg. [8]). It is assumed in the sequel that an algorithm for computing the electromagnetic fields in Ω is available. Thus, by integrating the system (1), the trajectory of an arbitrary electron is obtained.

In the sequel, it is assumed that the EM fields are time harmonic. If f is the frequency, the fields can be written as

$$\vec{E}(x,t)=\vec{E}(x,\omega)\sin\omega t, \quad \vec{B}(x,t)=\vec{B}(x,\omega)\cos\omega t,$$

where $\omega=2\pi f$ is the angular frequency.

Let us consider an electron leaving the boundary $\partial\Omega$ at the point x, the exit time being t. The exit time can be restricted to the period of one full harmonic oscillation of the field. Denoting by $\varphi=\omega t$ the phase of the field, we have

$$0\le\varphi<360^\circ.$$

What is more, it is assumed here that the initial velocity of for each electron is normal to the cavity wall and of constant size,

$$\vec{v}_0(x)=\vec{v}(x,0)=v_0\vec{n}(x), \quad v_0=\text{constant}.$$

Here $\vec{n}(x)$ is the interior unit normal at x. Typically, the value of v_0 is a few eV. Suppose that the electron is driven by the EM fields according to the system (1), and at the time $t'+nT>t$, it impacts the cavity wall at x' for the first time. Here, n is the number of full oscillation periods elapsed between the exit and first impact, and $0\le t'<T$. Defining the phase space as $X=[0,360^\circ[\times\partial\Omega$, we may define the *Poincaré map*, or the map of first return by

$$R: X\to X, \quad R(x,\varphi)=(x',\varphi'), \quad \varphi'=\omega t'.$$

This map turns out to be a useful tool in studying the multipacting.

We introduce some simple concepts related to the mapping R. A point $p=(x,\varphi)\in X$ is a *fixed point* of R, if

$$R(p)=p.$$

Similarly, a point p is an *n-periodic point* of R, if

$$R^n(p)=\underbrace{R\circ R\circ\ldots\circ R}_{n\text{ times}}(p)=p,$$

i.e., p is a fixed point of the n times iterated map. Obviously, a fixed point is also an n–periodic point, and more generally, if k is an integer factor of n, a k–periodic point is also an n–periodic point.

Let us divide the phase space X into an electron emitting and non-emitting parts by writing $X = G \cup W$, where

$$G = \{(x,\varphi) \in X \mid \vec{n}(x) \cdot \vec{E}(x,\varphi/\omega) \leq 0\},$$

$$W = \{(x,\varphi) \in X \mid \vec{n}(x) \cdot \vec{E}(x,\varphi/\omega) > 0\} = X \setminus G.$$

In other words, W consists of those points of the phase space where a free electron is immediately captured to the wall by the field while the electrons leaving G are injected into the cavity by the electric field. We assume here that the initial kinetic energy is negligible. The set G is called the *bright set*, while W is called the *shadow set*. The map R is defined in the shadow set as

$$R(p) = p, \quad p \in W.$$

The set of those points of G that after n iterations still are in the bright set is called an *n–bright set*, and denoted as

$$G^n = \{p \in G \mid R^n(p) \in G\} = \bigcap_{k=0}^{n} R^{-k}(G).$$

Before going to numerical examples of how these concepts can be used to track the multipacting, we need also another function. It is known that the onset of the multipacting process depends not only on the electron trajectories but also on the secondary electron yield at the walls. Therefore, suppose that the secondary electron yield at $x \in \partial\Omega$ is given by the function $\delta(x, E_{\text{kin}})$, where E_{kin} is the kinetic energy of the impacting electron. A typical curve $E_{\text{kin}} \mapsto \delta(x, E_{\text{kin}})$ obtained from the literature [4] is displayed in Figure 1.

Let us assume that an electron is emitted at $p = (x,\varphi) \in G$, and at the time of the impact the kinetic energy is $E_{\text{kin}}(p)$. We define the *multiplicity function* α as

$$\alpha : X \to \mathbb{R}, \quad \alpha(p) = \delta(x', E_{\text{kin}}(p)), \quad \text{where } R(p) = (x', \varphi').$$

Thus, the function α simply tells how many secondary electrons each initial electron in the phase space will introduce when impacting the wall. Note that in the shadow set we define naturally

$$\alpha(p) = 0, \quad p \in W.$$

Similarly, if p is a point of the n–bright set G^n, one can define an *n–multiplicity function* α_n counting the number of electrons that are launced by one single electron after n impacts. This function is

$$\alpha_n(p) = \alpha(p)\alpha(R(p))\alpha(R^2(p)) \ldots \alpha(R^{n-1}(p)).$$

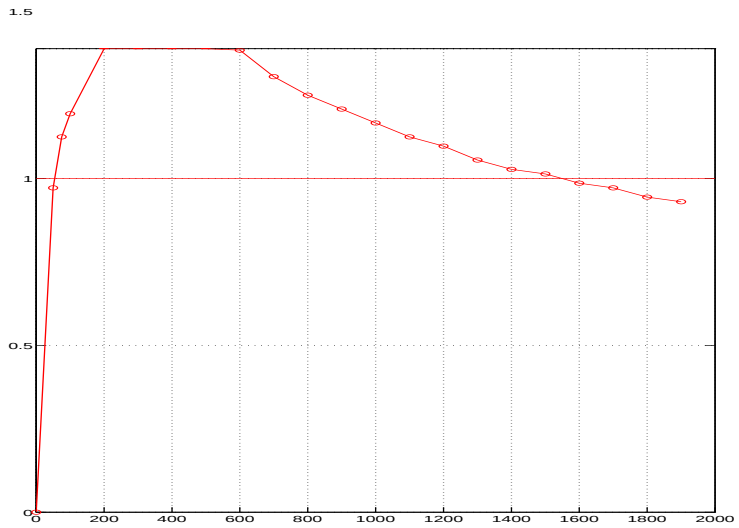

Figure 1. The secondary electron yield at different impact energies (in eV) for a niobium surface baked at 300°C

Our aim is to develop methods on one hand to recognize those EM field powers at which the electron multipacting may occur in the cavity. On the other hand, once a field power with potential multipacting has been found, it is important to understand the mechanism of the process. This includes the locating of the process in the phase space and the computation of the multipacting trajectories.

Let us first look at the latter problem. Assume that we are intersted in *one–point multipacting*: An electron emitted from the cavity wall returns after an integer number of complete oscillation periods of the EM field to the same point of the wall with a kinetic energy that will launch more than one secondary electrons. In terms of the mappings R and α, the corresponding phase space point must satisfy

$$R(p) = p, \quad \alpha(p) > 1,$$

i.e., p must be a fixed point in G with the multiplicity function greater than one. To search for the fixed points, we may look at the distance function d_1, defined as

$$d_1(p) = \sqrt{|x - x'|^2 + \gamma^2 |e^{i\varphi} - e^{i\varphi'}|^2}, \quad \text{where } p = (x, \varphi) \text{ and } (x', \varphi') = R(p).$$

Here, $|x - x'|$ is the Euclidean distance of the points x and x' and γ is an appropriately chosen constant. It will be fixed in the numerical examples later on. The possible one–point multipacting points are among the minima of the function d_1, and at those points, $d_1(p) = 0$. Due to the numerical errors in the trajectory calculations, the criterion for a fixed point should be relaxed as $0 \le d_1(p) < \varepsilon$, $\varepsilon > 0$ being a chosen tolerance. What is more, the minimum search must be restricted to the area where $\alpha(p) > 1$. The *order* of the multipacting process is defined as the number of full oscillation periods T of the EM fields elapsing between primary electron emission and the first impact.

Similarly, the *two–point multipacting* points, and more generally, the *n–point multipact-*

ing points can be located. They correspond to those minima of the function

$$d_n(p) = \sqrt{|x - x'|^2 + \gamma^2 |e^{i\varphi} - e^{i\varphi'}|^2}, \quad p = (x, \varphi) \text{ and } (x', \varphi') = R^n(p),$$

where

$$0 \le d_n(p) < \varepsilon, \quad \alpha_n(p) > 1.$$

Note that each one–point multipacting is bound to minimize also the distance function d_n, too, so in order to differentiate between the different multipacting processes the trajectories must be checked. The order of an n–point multipacting process can be defined as the number of full oscillation periods elapsing in completing the full cycle of n impacts.

As mentioned above, an important question is also whether a multipacting process is possible at a given input power of the EM fields. Therefore, one needs an effective sweeping method with respect to the field power. To this end, assume that the field power P is fixed for a while. Choose a number of points p_ℓ of G, $1 \le \ell \le L$, either randomly or by using a grid. From each point, launch one spontaneously emitted electron and let the system run for a while. After a chosen number N iterations of the map R, count how many electrons still remain in the bright region, i.e., compute the number

$$c_N(P) = \text{number of } \{p_\ell : R^N(p_\ell) \in G\}.$$

If the points p_ℓ are chosen densely enough, the distribution of those points p_ℓ that contribute to the sum above gives a good image of the N–bright set G^N. Repeating this electron count for different values of the power P and plotting the function $P \mapsto c_N(P)$, one should be able to recognize the values of P where the multipacting is likely to occur: They should stand out as those values where $c_N(P)$ is relatively large. Notice that in this sweeping scheme it is assumed that the physical multipacting occurs only if a periodic point of R is not strongly repelling. Obviously, if the map R has an isolated fixed point or n–periodic point p_0 such that all the neighboring points are quickly drifted away to the shadow set, this type of electron counter will not be able to find it. However, if the point has a stable basin from which all the electrons drift toward the point p_0, the number $c_N(P)$ remains clearly positive.

3 Numerical experiments with a coaxial cable

The ideas developed in the previous section are demonstrated here in a simple but quite important geometry. The cavity Ω is a coaxial line with totally reflecting ends. The frequency is adjusted so that the electric field in the TEM mode forms a standing wave. More precisely, let a and b denote the inner and outer radii, respectively, and h the length of the cavity. If f is the frequency and U is the voltage drop between the inner and outer radius, the electric and magnetic fields are given by the formulas

$$\vec{E}(x,t) = \frac{U}{r \log(b/a)} \sin kz \sin \omega t \; \vec{e}_r = \frac{U}{2r \log(b/a)} (\cos(kz - \omega t) - \cos(kz + \omega t)) \; \vec{e}_r$$

$$\vec{B}(x,t) = \frac{U}{cr \log(b/a)} \cos kz \cos \omega t \; \vec{e}_\theta = \frac{U}{2cr \log(b/a)} (\cos(kz - \omega t) + \cos(kz + \omega t)) \; \vec{e}_\theta$$

Here, $k = \omega/c = 2\pi/\lambda$ and (r, θ, z) is the representation of the field point x in cylindrical coordinates, the origin being fixed at the left end of the axis of the cavity. In our model calculations, we use the frequency $f = 1.3$ GHz, and the dimensions of the cable are $2a = 1.74$ cm, $2b = 4.0$ cm, the impedance thus being about 50 Ω. The length h of the cavity is assumed to be $h = 2\lambda = 46.12$ cm. From the equations (1) governing the dynamics, it is easy to see that the analysis may be restricted to the plane $\theta = 0$. Thus the problem is spatially two-dimensional.

Let us start with the problem of finding those field powers that allow a possible multipacting in the cavity. The average (incident) power flow P of the field is related to the voltage U through the formula

$$P = \frac{\pi U^2}{4\eta \log(b/a)},$$

where η is the wave impedance of the vacuum. In our experiment, we search for a multipacting starting at the outer shell $r = b$. By the symmetry of the problem, the consideration is restricted to the segment between the maximum and minimum of the electric field. Let the z–coordinate of the leftmost maximum of the electric field be at $z = z_{\min}$, and the adjacent minimum at $z = z_{\max}$. With the dimensions fixed as above, we have $z_{\min} = \lambda/4 = 5.77$ cm and $z_{\max} = \lambda/2 = 11.53$ cm. Hence, it is assumed that $z_{\min} \le z \le z_{\max}$. What is more, the phase φ may be restricted to the interval $[0, 180°[$. The remaining rectangle $[z_{\min}, z_{\max}] \times [180°, 360°[$ is in the shadow set W as one can easily check. In our example, we pick the grid points in the bright rectangle $[z_{\min}, z_{\max}] \times [0, 180°[$ as

$$p_{k,\ell} = (z_k, \varphi_\ell), \quad \text{where} \quad \begin{cases} z_k = z_{\min} + \dfrac{k}{K}(z_{\max} - z_{\min}) = \dfrac{(K+k)\lambda}{4K}, & 0 \le k \le K, \\ \varphi_\ell = \dfrac{\ell}{L} 180°, & 0 \le \ell < L. \end{cases}$$

The numbers K and L are chosen as $K = 19$, $L = 91$, yielding 1800 gridpoints. With this grid, the function c_N is computed. The field power is alowed to vary from 0 to 1000 kW, the step length being 0.5 kW. The P versus c_N plot is shown in Figure 2 for $N = 10$, $N = 20$ and $N = 30$. The map R is calculated by solving the system (1) using 2th and 3th order Runge–Kutta-Fehlberg ODE solver ([5]). The initial velocity v_0 is chosen $v_0 = 2$eV. The plot shows clear power intervals where the spontaneously emitted electrons do not drift quickly to the shadow region. Notice also that beyond the field power $P = 800$ kW, no multipacting phenomena (visible by the described algorithm) seem to occur. One should observe that in Figure 2, the multiplying effect of the secondary electron yield has not been taken into account in any way. This effect is briefly discussed later.

To gain more insight into the dynamics, let us take a look at a typical value of P where the multipacting seems possible. We choose $P = 650$ kW. In Figures 3a–3d, we have plotted a gray scale topographic image of the distance functions d_1 and d_{10}, and the multiplicity functions α_1 and α_{10}, respectively. The value of the constant γ was chosen as $\gamma = (L-1)\lambda/(4\pi K) = 8.69$ cm so that one discretization step in phase direction

affects d_n roughly as much as one in the distance direction. In the distance function plot, the minima correspond to the darkest shading. Moreover, in the plot 3c of d_{10}, those pixels that have drifted to the shadow region before the 10th iteration are marked with white. Hence, the tinted area in the d_{10} plot represents the n–bright region G^n with $n = 9$ at the present discretization level. In the plots 3b and 3d of the multiplicity functions α_n, the maxima correspond to the darkest shading, and pixels where $\alpha_n < 1$ (i.e. no multipacting possible) have no shading. Thus, the tinted area in the α_n plots provide a mask for reading the distance function plots.

It is informative to look at the dynamics generated by the map R in the phase space X. Consider four different values of the power where the c_N plot indicates the presence of multipacting, $P = 650$ kW, $P = 610$ kW, $P = 500$ kW and $P = 405$ kW. Figures 4a–4d present the images of 500 randomly chosen points in a rectangle $[\lambda/4, (1 + 0.25)\lambda/4] \times [0°, 100°]$ in the phase space after ten iterations of the map R. Those electrons that are at the inner shell $r = a$ are marked with an asterisk while those at the outer shell $r = b$ correspond to circles. Two characteristic phenomena should be observed here. Firstly, all the points off the maximum of the electric are slowly drifted away from the maximum of the field, and eventually they hit the shadow region and die off. Secondly, the process is strongly phase-focusing, i.e. all the electrons near the electric maximum are clustered to well defined phase values. Thus, there are points that are weakly repelling in the spatial direction but weakly attractive in the phase direction.

Motivated by this observation, we compute a different multipacting indicator. This time, we restrict the grid points to the maximum of the electric field only, i.e., we search for multipacting at $z = \lambda/4$. Let the grid points p_ℓ be

$$p_\ell = (z_{\min}, \varphi_\ell), \quad \varphi_\ell = \frac{\ell}{L} 180°, \quad 0 \le \ell < L.$$

Again, we have $L = 91$. Figures 5a–5c display the functions $c_N(P)$ with $N = 10$, $N = 20$ and $N = 30$ obtained with this grid. Clearly, there is a clear correlation with the previous plots in Figure 2, since the maximum of the electric field is the dominant location for the phenomenon.

With this new grid, we perform yet another experiment that turns out to be very informative. We compute the distance function d_{30} for different values of the power. Notice that in this case, the spatial variable z is kept fixed, so the distance function depends on one single variable, the phase. This enables us to plot the distance function in the power versus phase plane as a topographic image. Figure 6 depicts a gray scale landscape of d_{30}. Again, white areas indicate those points that have drifted to the shadow region, and the darkest areas mark the minima.

In this picture we see an intersting self–similarity: some of the patterns repeat themselves shifted and dilated. In fact, a closer study of the electron orbits producing the patterns show that the similar patterns arise from the same type of orbits having only different order. Based on this plot, several distinct potential multipacting processes can be identified.

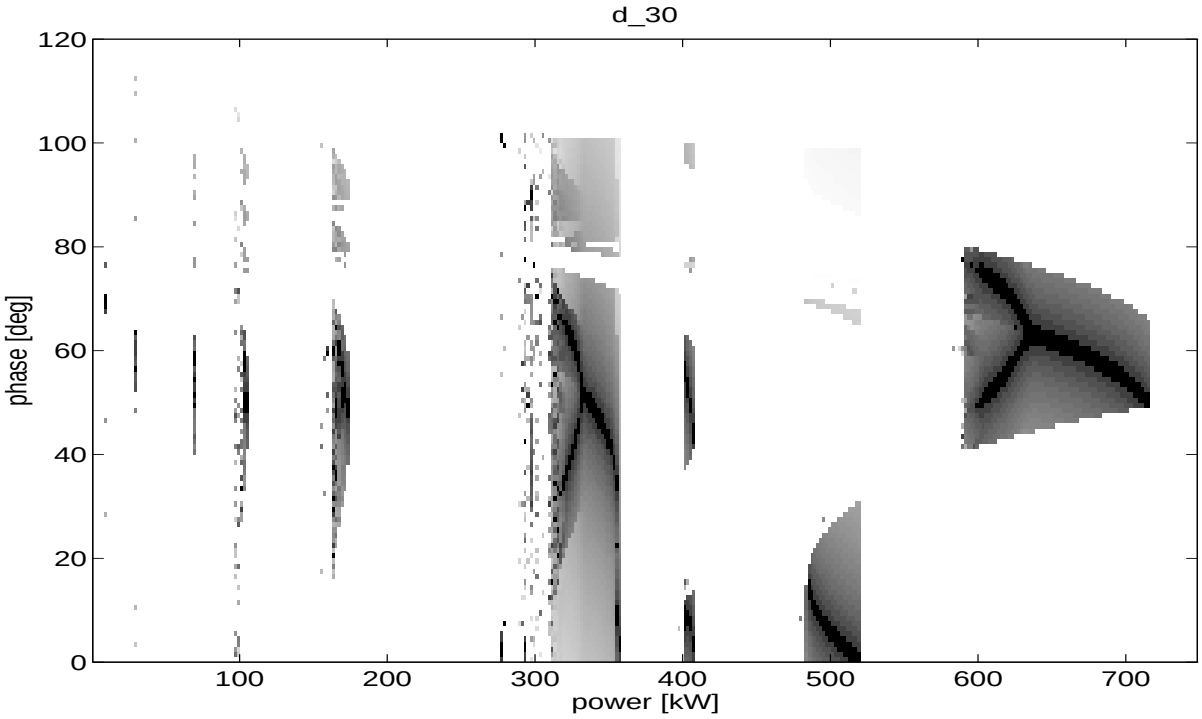

Figure 6. The gray scale contour plot of the distance function d_{30} when the primary electron emission is restricted to the maximum of the electric field. The darkest shading corresponds to the minima. Initial phases corresponding to electron trajectories that end up to the shadow are marked with white.

Consider first the power interval 580–720 kW. From this interval, we pick two typical sample powers. First, let $P = 650$ kW. At this field power, the distance function has a single minimum at $\varphi = \varphi_0 = 62°$. The distance function is plotted in Figure 7a. Figure 8a shows the electron trajectory starting at the location of the minimum. Clearly, the trajectory is very accurately synchronous to the EM field, and it seems to correspond a first order one–point multipacting. Next, consider the field power 610 kW. At this power, the distance function has two separate minima at $\varphi = 54°$ and $\varphi = 74$, see Figure 7b. The electron trajectory in this case turns out to be more complicated than in the previous case. In Figure 8b, the orbit starting at $\varphi_0 = 54°$ is plotted. We see that the first electron touchdown takes place not at the same phase as where the trajectory started but at the second minimum, $\varphi = 74°$. Thus, the two minima do not correspond to two separate synchronous trajectories but rather to a more complicated process of order 1+1.

The power interval 480–520 kW is next under consideration. Figure 7c shows the distance function profile and Figure 8c depicts the trajectory of the electron at 500 kW, starting at the phase $\varphi_0 = 6°$ corresponding to the minimum of the distance function. The trajectory in this case is a "pitch–catch" trajectory starting at the outer shell of the cable, hitting the inner shell at the phase $\varphi = 224°$ and returning after one cycle of the EM field. The behavior could be anticipated by Figure 4c. The process is roughly

of the order $2/3 + 1/3$.

Finally, let us look at the distance function 7d, which corresponds to a composite trajectory in Figure 8d, found at the field power 405 kW. The trajectory consists of one outer–to–outer round trip plus one pitch–catch round trip. Here the touchdown phases are $\varphi = 49°$, $\varphi = 7°$ and $\varphi = 249°$ at the inner shell. The order is $2+2/3+1/3$.

The distance function plots in Figure 7 give some idea of the stability of the synchronous trajectories. Around the synchronous phase, there is a neighborhood where the distance function d_{30} is linear. this means that all the electrons that started in this sloped region around the synchronous phase have glided to the attracting phase. In terms of dynamical systems, we might call the sloped regions the basin of the attractor. Since the primary electron emission is a random process, we may deduce that the larger the basin is the more likely the onset of the multipacting is.

In our analysis so far, the emphasis has been mostly on the stability of the trajectories. To obtain the full picture, the secondary electron yield must be taken into consideration. For some stable trajectories, it may be prohibitively low for multipacting. In Figure 9, we have plotted the counter function $c_{30}(P)$ appearing in Figure 5c, but this time each electron is counted according to the multiplicity describing how many secondary electrons it has caused after 30 impacts. If the kinetic energy passes the window where the secondary electron yield is large, the enchancement is considerable. We see that the effect of the multiplicity function is quite dramatic.

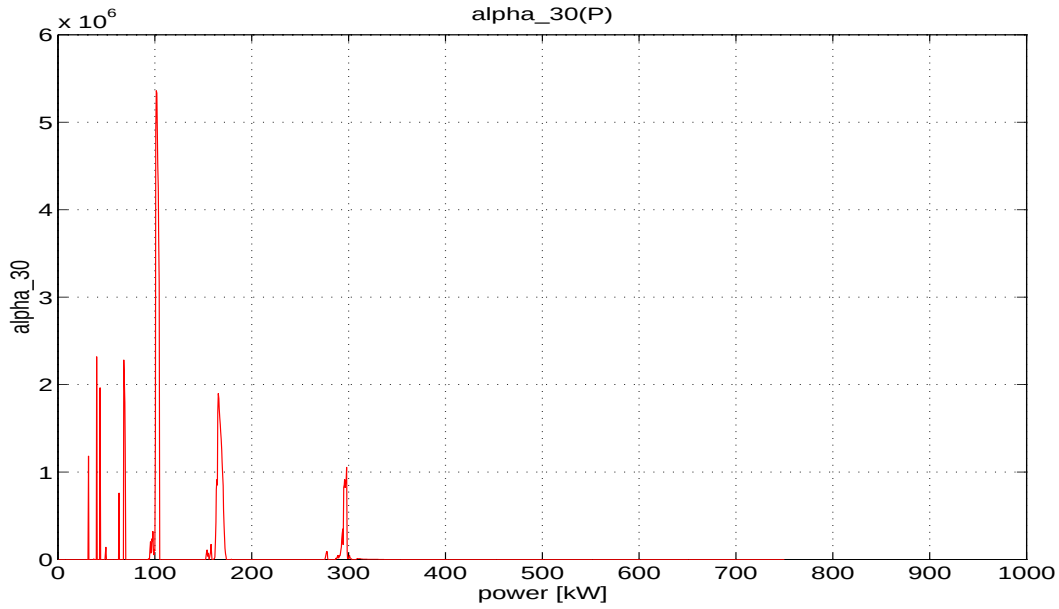

Figure 9. The electron counter c_{30} of Figure 5c, each electron being enchanced with the corresponding multiplicity function α_{30}.

Finally, we examine the question whether the multipacting phenomena described above obey some simple scaling laws. The first natural question is what the ratios of the field intensities are corresponding to the same multipacting process of different order. In the one–point multipacting case in cylindrical cavities as well as that between two parallel

plates, the field levels scale inversely proportionally to the multipacting order ([1],[4]). To answer this question in the case of a coaxial line, one has to identify multipacting processes belonging to the same family with different order. For this somewhat ambiguous identification, Figure 6 is quite suggestive. We pick the shaded regions with the dark minima forming a Y–shaped valley. This shape seems to repeat itself in the picture. At the present discretization level, only two are clearly visible. By using a finer grid, one can find more of them at lower field powers. As it was pointed out in the discussion above, each one of these regions correspond to basically two different multipacting process, depending on whether the distance function has one or two minima. In Tables 1a–1b, we have listed six of the power intervals where the one point process occurs and four of those where the process with two minima occur, and by checking from the trajectory calculations, the orders of the corresponding multipacting orbits are listed. In Figure 10, the maxima of the electric field at the outer shell are plotted versus the inverse of the order plus one. Note that the electric field maximum is related to the field power by the formula

$$E_{\max} = \frac{1}{b}\sqrt{\frac{4\eta P}{\pi \log(b/a)}}.$$

The dependence of the electric field maximum is roughly linear, i.e.,

$$E_{\max} \sim \frac{1}{n+1}.$$

Single minimum process		
Order	Power ($[P]$ =kW)	Phase
1	631–715	50°–65°
2	332–353	40°–55°
3	169–173	50°–60°
4	103–104	50°–65°
5	68	60°
6	49	60°

Double minimum process		
Order	Power ($[P]$ =kW)	Phase
1+1	600–630	50°–80°
2+2	320–331	40°–70°
3+3	166–168	50°–60°
4+4	102–103	50°–65°

Next, we check the effect of changing the frequency f of the field. We compute the function $c_N(P)$ plotted in Figure 5 with several frequencies. It turns out that at different frequencies, the functions c_N are dilated copies of each other, i.e., the shape of the function is affected negligibly by the frequency scaling. Therefore, the power shift of the multipacting phenomena is easily tractable. We choose the one–point multipacting trajectory shown in Figure 8a as the reference case. The higer order order multipacting processes belonging to the same family were given in Table 1a. In Figure 11a, we have plotted the shift of these multipcating processes when computed with four different frequencies. The frequencies used are 0.65 GHz, 1.3 GHz, 1.95 GHz and 2.6 GHz. The vertical axis gives the square root of the peak value of the electric field at the outer shell of the line. The dependence seems to follow a linear rule, i.e., at multipacting

RF powers, the value of the electric field seems to be proportional to the RF frequency squared.

The effect of geometric dimensions of the coaxial line is studied in the similar fashion. Let both the inner and outer diameter of the line vary so that the impedance of the line remains unaltered, i.e., b/a =constant. Similarly to the previous case, we may locate the multipacting RF powers of different order. Figure 11b depicts the shift of the peaks when both a and b were scaled by a factor 0.5, 1, 1.5 and 2. The horizontal axis is the outer radius of the line, the vertical axis is the peak value of the electric field at the outer shell. The dependence is again linear.

We may summarize the scaling laws obtained so far in the following fashion: Let d denote a size parameter of the coaxial line, i.e., $a = \alpha d$ and $b = \beta d$, where α and β are dimensionless shape parameters of the line, $\alpha < \beta$. The maximum value $E_{\max}$ of the electric field when multipacting occurs depends on the RF frequency f, the size parameter d and the order of the multipacting as

$$E_{\max} \sim \frac{f^2 d}{n+1},$$

In terms of the input power of the line, the scaling rule translates

$$P_{\text{input}} \sim \frac{d^4 f^4}{(n+1)^2}.$$

This scaling law agrees with the experimental ones found by Woo in [6].

4 Conclusions

The concepts arising from the theory of dynamical systems seem to provide effective tools for analyzing the multipacting phenomenon. The use of the general theory developed for dynamical systems (see e.g. [2]) is still quite limited in this work, and we believe that the analysis can be developed much further by using e.g. probality densities in connection with supeconducting structures.

The present work is aimed mainly to develop and to demonstrate the general ideas how to find multipacting levels. In forthcoming works, the ideas will be applied to more specific geometries. In particular, while the scaling laws give some idea of the multipacting levels as functions of different parameters, the multiplicity functions do not scale according to any simple scaling law. Therefore, a complete analysis of the multipacting levels in a given geometry requires always some recalculations.

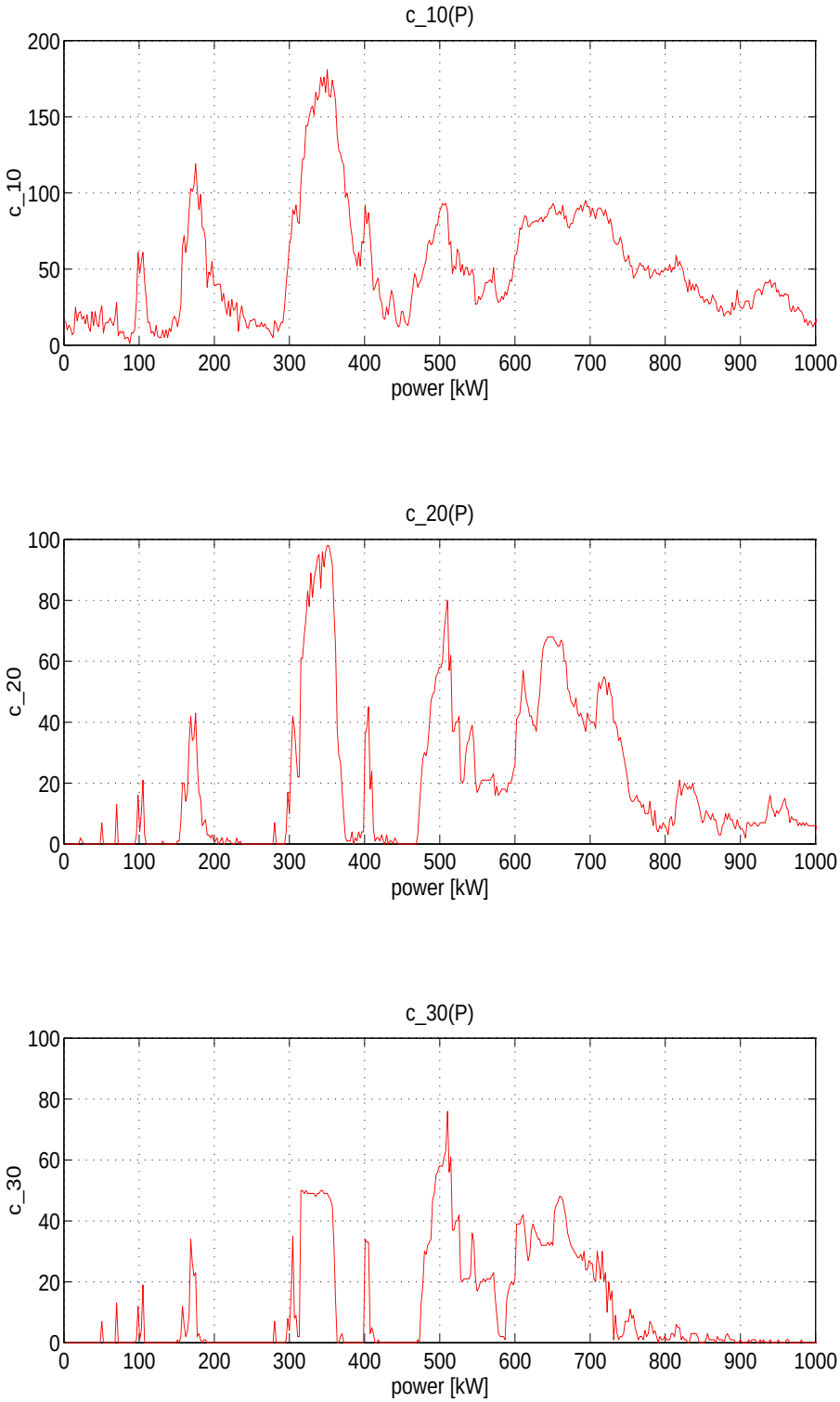

Figure 2. The electron counter function $c_N(P)$ at different RF field powers with $N = 10$, $N = 20$ and $N = 30$. The initial number of electrons was 1800, and $c_N(P)$ gives the number of the electrons remaining in the bright region after N iterations.

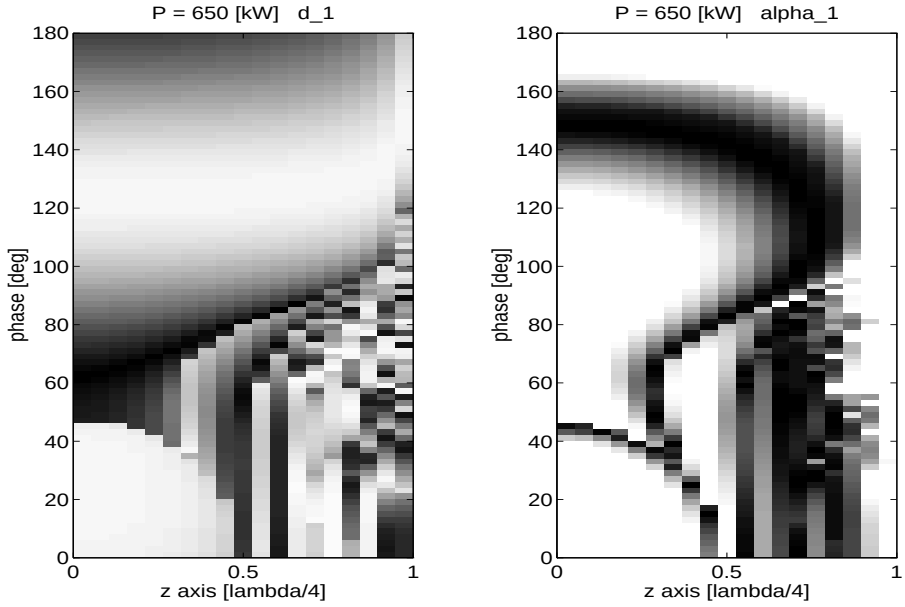

Figure 3a–3b. The distance map d_1 at the RF field power 650 kW at the outer shell of the coaxial line (Fig. 3a). The horizontal axis is the distance from the maximum of the electric field in units $\lambda/4$, the vertical axis is the phase. The darkest shading corresponds to minima. The corresponding multiplicity function α_1 is is plotted in the same coordinates (Fig. 3b). Here, the darkest shading corresponds to maxima. White areas indicate that $\alpha_1 < 1$. In this example, the secondary electron yield at the maximum of the electric field is prohibtively low for multipacting.

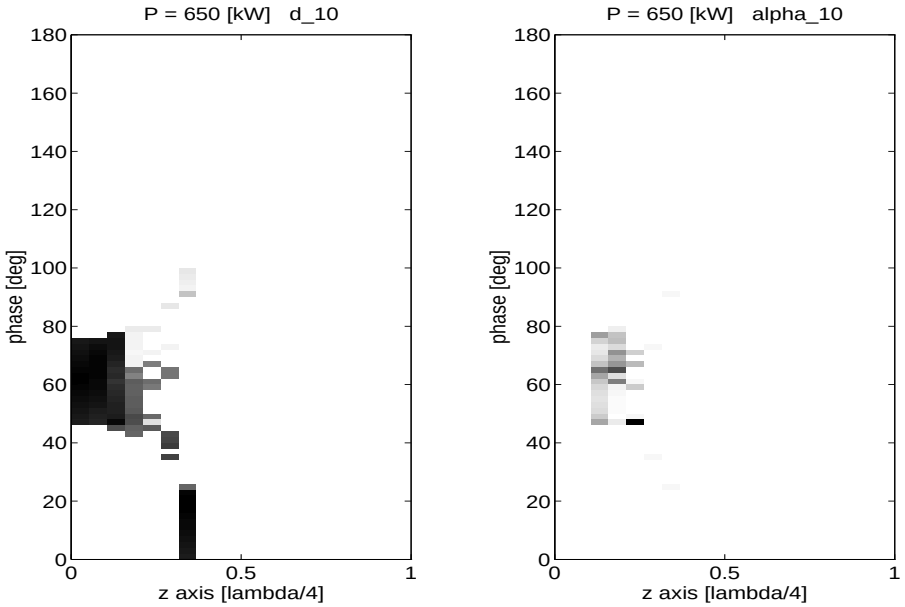

Figure 3c–3d. The distance map d_{10} (Fig. 3c) at 650 kW and the multiplicity function α_{10} (Fig. 3d). In the distance function plot, the white areas are those points that have ended up to the shade region.

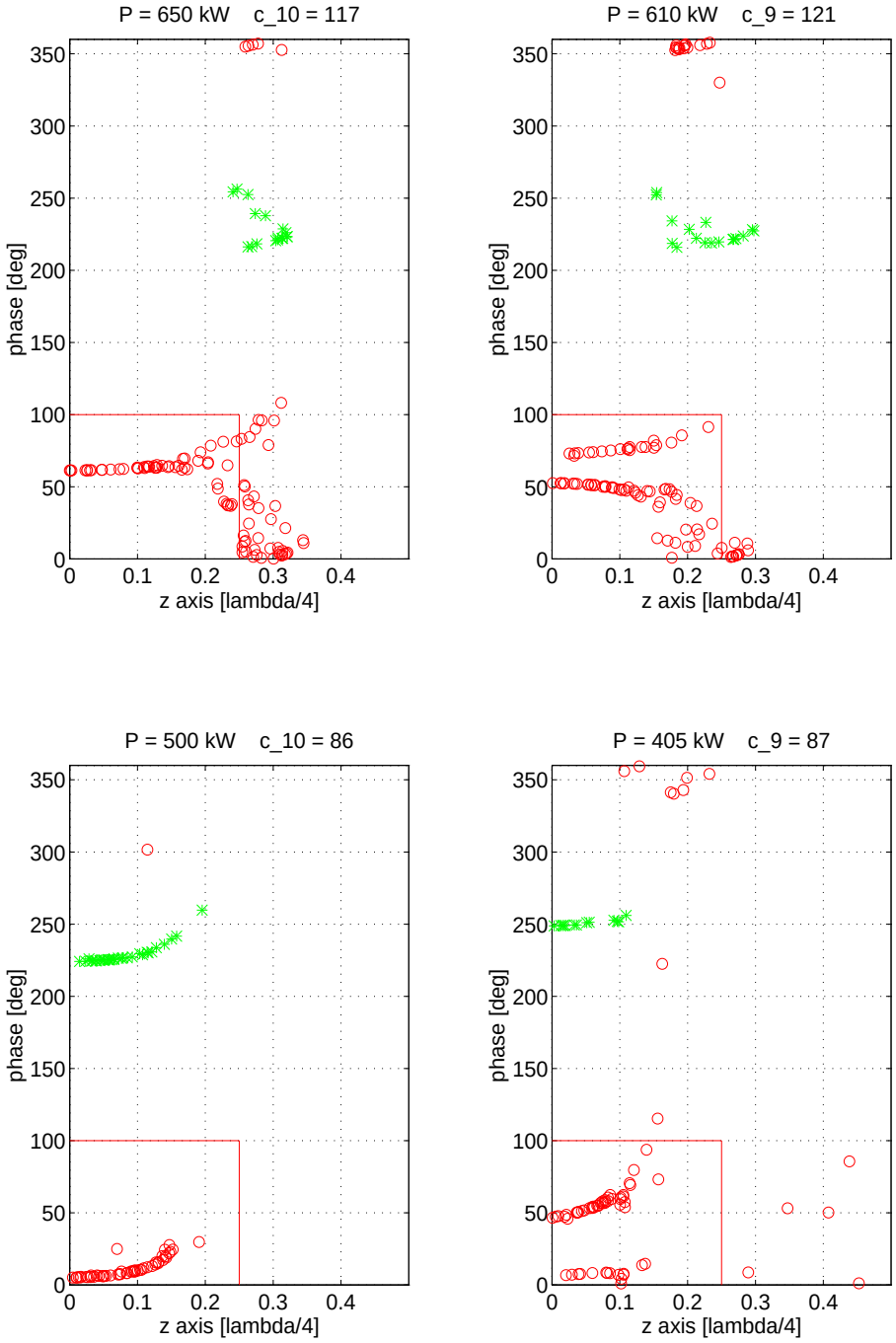

Figure 4. The dynamics generated by the Poincaré map R. The figures represent the locations of 500 randomly chosen points in the enchanced rectangle after 10 iteration steps at different RF powers. The points in the outer shell are marked with a circle, the ones in the inner shell with an asterisk. The points that have drifted to the shadow region before the tenth iteration are omitted.

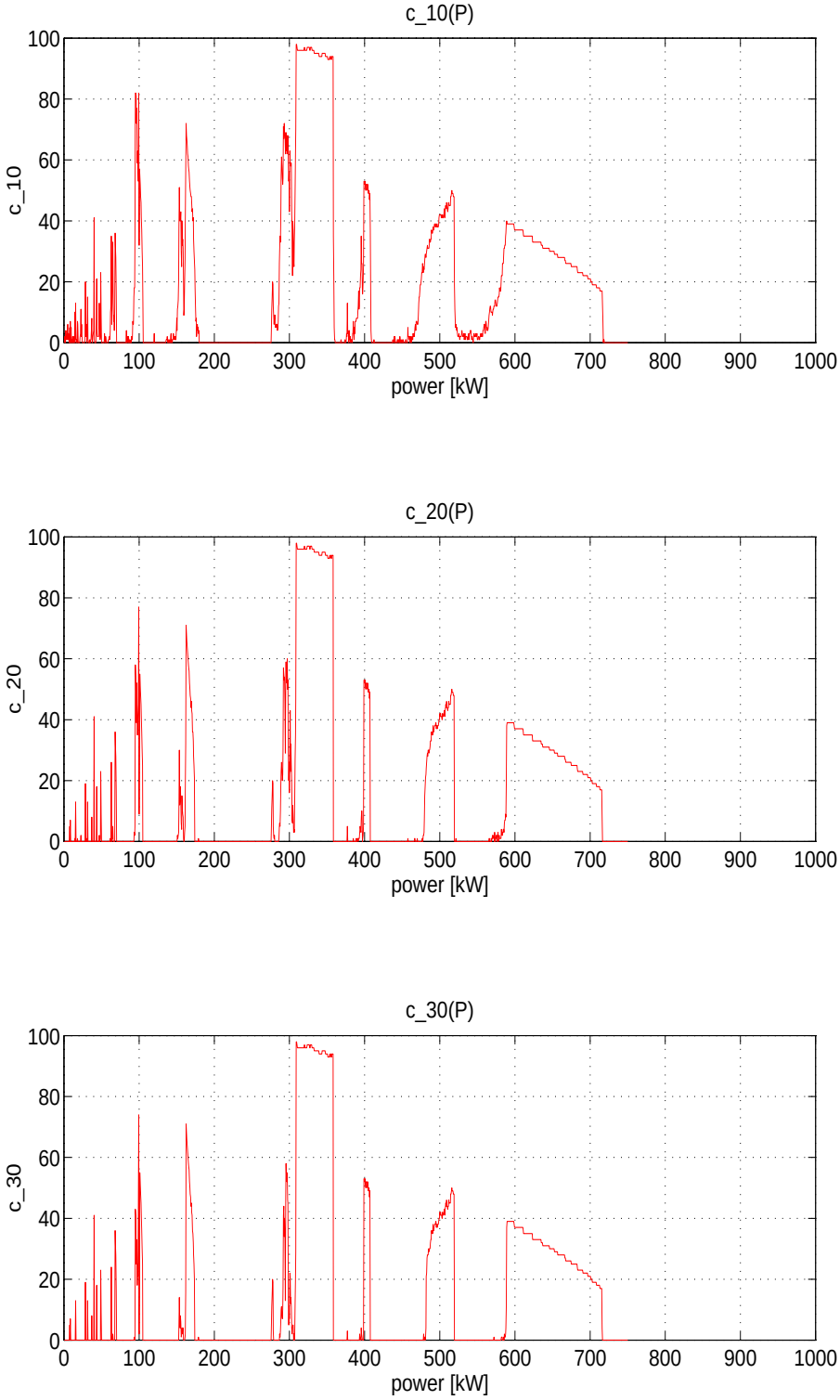

Figure 5. The electron counter function $c_N(P)$ with electrons restricted to the maximum of the electric field. As in Figure 2, we have $N = 10$, $N = 20$ and $N = 30$. The initial number of electrons was 90, and $c_N(P)$ gives the number of the electrons remaining in the bright region after N iterations. Notice the similarity with Figure 2.

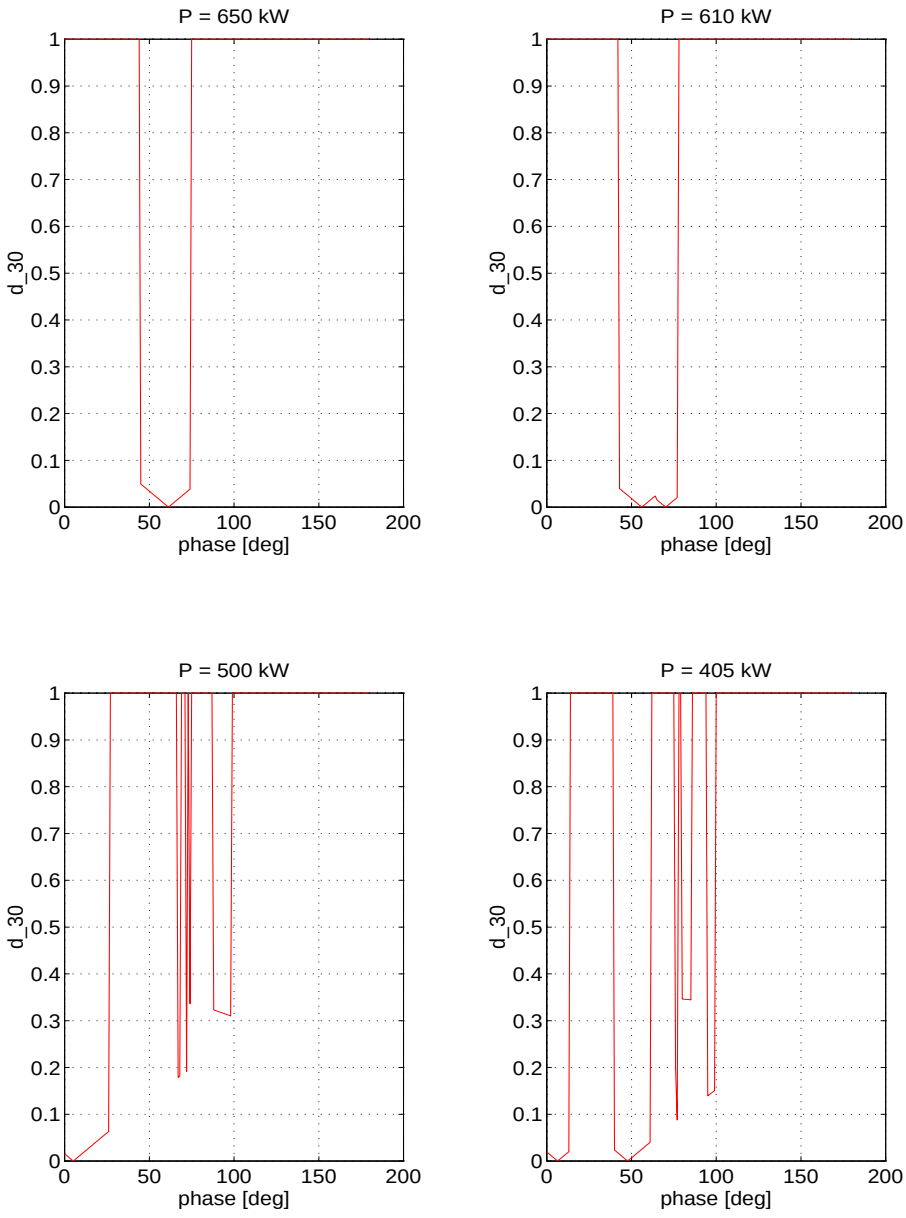

Figure 7a–7d. The distance functions d_{30} for different RF powers at the maximum of the electric field. The synchronous trajectories correspond to those phases where the distance function vanishes. Electrons with the initial phase in the neighborhood where the distance function is linear have drifted to the synchronous trajectory.

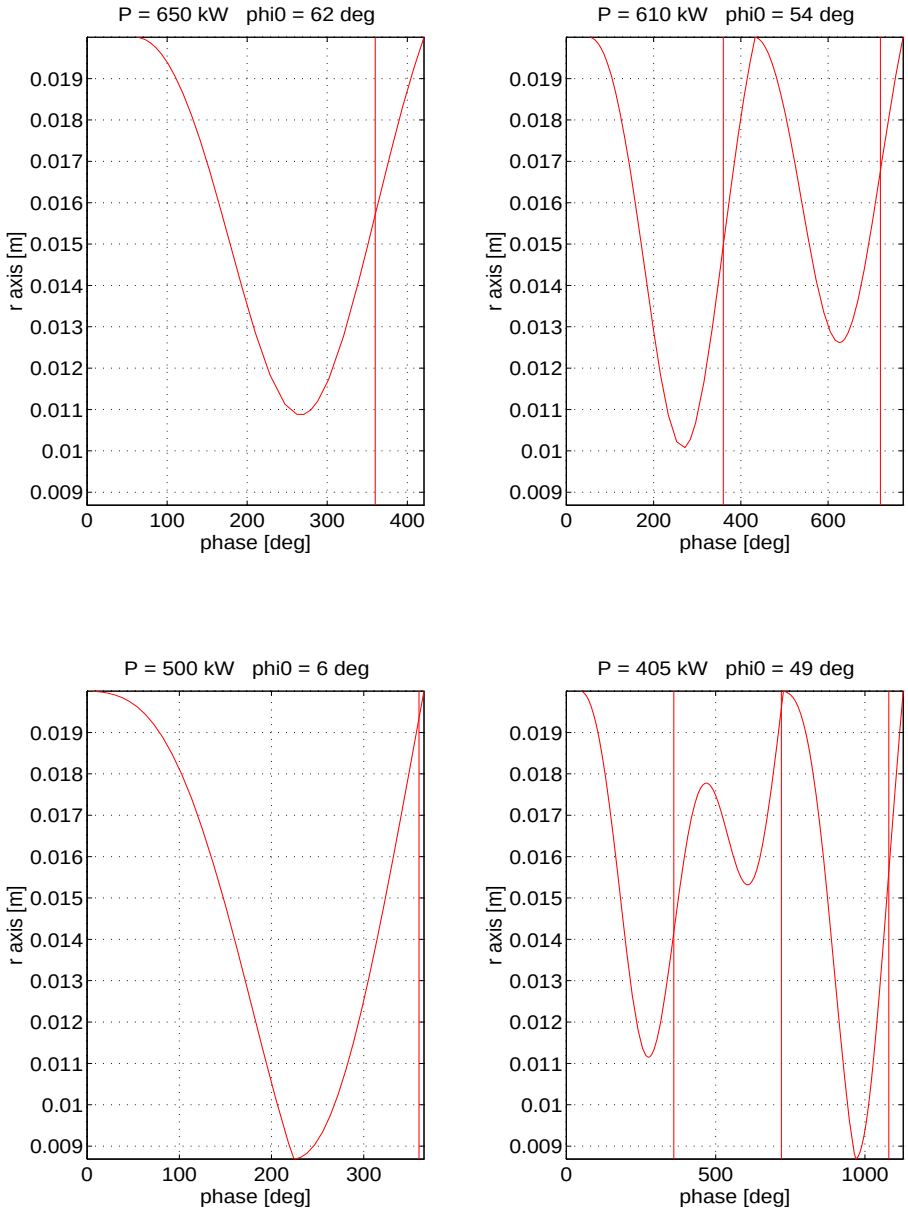

Figure 8a–8d. The synchronous electron trajectories starting at the minima of the distance function. The RF powers coincide to those in Figure 7.

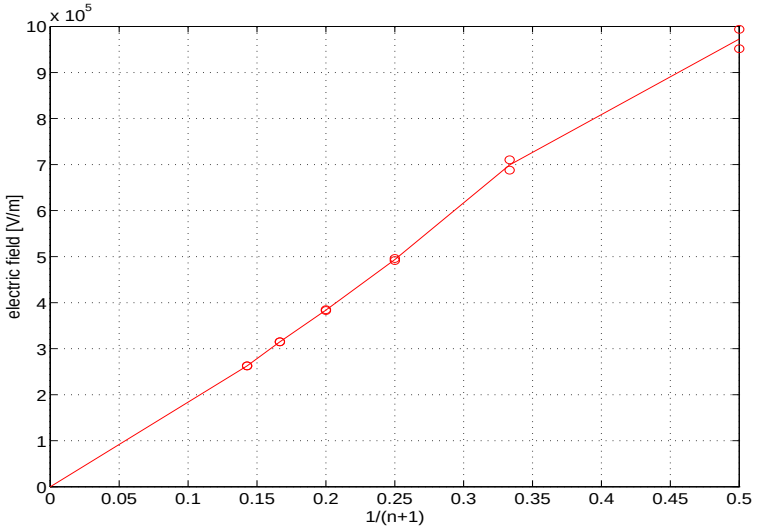

Figure 10. The peak values of the electric field at the outer shell of the coaxial line. The horizontal axis is $1/(n+1)$, where n is the order of the multipacting. The circles indicate the widths of the multipacting bands.

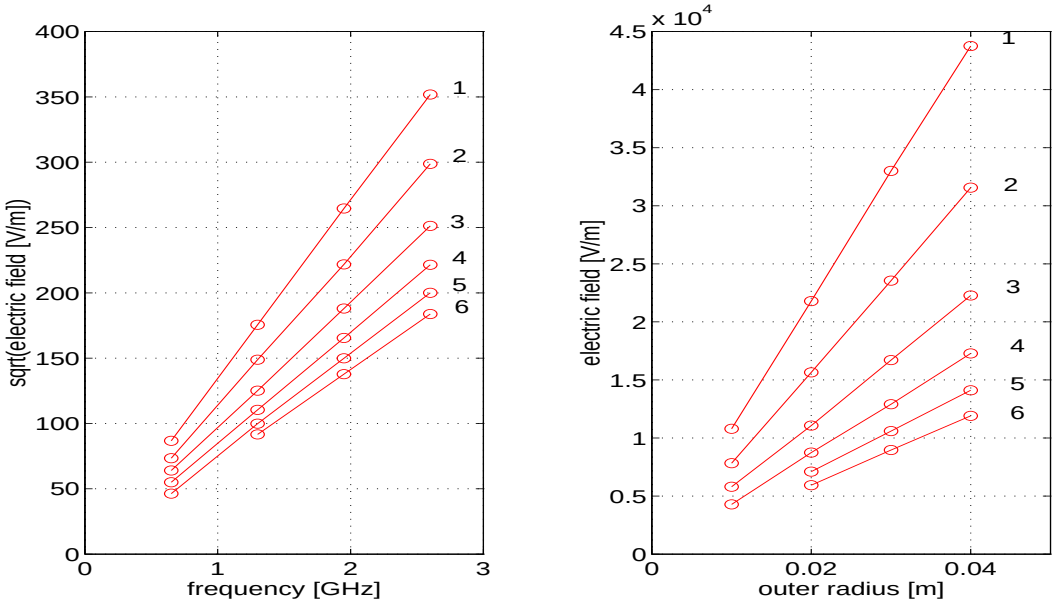

Figure 11a–11b. In Figure 10a, the curves represent the effect of varying the RF frequency. In the experiment, the radial dimensions of the coaxial line were kept fixed. The labels indicate the order of the multipacting, and the curve indicates the square root of the peak value of the electric field at the outer shell at which the multipacting occurs. In the experiment of Figure 10b, the RF frequency is fixed and the radial dimensions of the coaxial line are changed, keeping the impedance of the line fixed, i.e., the ratio of the inner and outer radius is unaltered. The horizontal axis is the radius of the outer shell, the vertical one square root of the maximum of the electric field at the outer radius.

Acknowledgements: The authors wish to thank Prof. Jukka Sarvas for very useful and enlightening discussions. The collaboration of The Research Institute of High Energy Physics, University of Helsinki (SEFT) and especially Dr. Esko Pietarinen is acknowledged.

References

[1] U. Klein and D. Proch: Multipacting in superconducting RF structures. Talk presented at the *Conference on Future Possibilities for electron Accelerators*, Charlottesville 1979. WU B 78–34.

[2] A. Lasota and M. Mackey: *Chaos, Fractals and Noise.* Springer Verlag Applied Mathematical Sciences 97, New York 1994.

[3] C. M. Lyneis, H. A. Swettman and J. P. Turneaure: Elimination of electron multipacting in superconducting structures for electron accelerators. Appl. Phys. Lett. **31** (1977) 541–543.

[4] Piel, H.: Superconducting cavities. In: *Proceedings of the CERN Accelerator School: Superconductivity in Particle Accelerators*, Geneva 1989, 149–196.

[5] J. Stoer and R. Bulirsch: *Introduction to Numerical Analysis.* Springer Verlag, New York 1983 (2nd ed.)

[6] R. Woo: Multipacting Discharges Between Coaxial Electrodes. J. Appl. Phys. **39** (1968) 1528–1533.

[7] J. Tuckmantel: One Point Multipacting Levels Determined without Electron Tracking. In: *European Organization for Nuclear Research series notes*, 1 August 1989, 569–579.

[8] L.P. Landau, E.M. Lifshitz: *Course of Theoretical Physics* Volume 2. Pergamon 1976.